VOL. 15, NO. 19, OCTOBER 2020 ISSN 1819-6608
ARPN Journal of Engineering and Applied Sciences

www.arpnjournals.com

RECOVERY OF ASTEROIDS FROM OBSERVATIONS OF TOO-SHORT ARCS BY TRIANGULATING THEIR ADMISSIBLE REGIONS

Daniela Espitia and Edwin A. Quintero
Observatorio Astronómico, Universidad Tecnológica de Pereira, Complejo Educativo La Julita, Risaralda, Colombia
E-Mail: equintero@utp.edu.co

ABSTRACT

The data set collected during the night of discovery of a minor body constitutes a too-short arc (TSA), resulting in failure of the differential correction procedure. This makes it necessary to recover the object during subsequent nights to gather more observations that will allow a preliminary orbit to be calculated. In this work, we present a recovery technique based on sampling the admissible region (AdRe) by the constrained Delaunay triangulation. We construct the AdRe in its topocentric and geocentric variants, using logarithmic and exponential metrics, for the following near-Earth asteroids: 3122 Florence, 3200 Phaethon, 2003 GW, 1864 Daedalus, 2003 BH84 and 1977 QQ5; and the main-belt asteroids: 1738 Oosterhoff, 4690 Strasbourg, 555 Norma, 2006 SO375, 2003 GE55 and 32811 Apisaon. Using our sampling technique, we established the ephemeris region for these objects, using intervals of observation from 25 minutes up to 2 hours, with propagation times from 1 up to 47 days. All these objects were recoverable in a field of vision of 95' x 72', except for 3122 Florence and 3200 Phaethon, since they were observed during their closest approach to the Earth. In the case of 2006 SO375, we performed an additional test with only two observations separated by 2 minutes, achieving a recovery of up to 28 days after its discovery, which demonstrates the potential of our technique. We implement our recovery technique in a web service available at http://observatorioenlinea.utp.edu.co/recoveryservice/.

Keywords: admissible region, asteroids, astrometry, ephemerides.

1. INTRODUCTION

The orbital dynamics of minor bodies of the solar system is a current area of interest in astronomy, especially when these are newly discovered objects for which there are no previous records. Different observatories around the world report the finding of these objects on a daily basis, but due to the short interval of observation (*too-short arcs, TSA*), the astrometric data collected are not sufficient to establish a preliminary orbit (Gronchi, 2004). This is because the classic methods of initial orbit determination fail in this type of case (Milani and Knežević, 2005).

In order to establish a preliminary orbit for new objects, it is necessary to ensure their reobservation following the nights after the discovery. This task requires anticipating their predicted location in the celestial sphere, a procedure known as *recovery* (Milani, 2001; Milani and Gronchi, 2009). The utility available on-line known as *New Object Ephemerides*[1] is a service offered by the MPC (Minor Planet Center) for the recovery of new objects. However, this service is based on ephemeris calculation via the orbit-fitting procedure by Väisälä (Gwyn, Hill, and Kavelaars, 2012), which is a classic method that provides acceptable results for main-belt asteroids (MBAs) but not for near-Earth asteroids[1] (NEAs). In addition, this fitting applies the approximation of assuming that the object is observed at its perihelion (Väisälä, 1939; Kristensen, 2006).

In contrast to classical methods, Milani *et al.* (2004) uses the concept of the *admissible region* (AdRe) to delimit the location region of an asteroid seen from Earth, followed by triangulation sampling within this region to anticipate the recovery. While in the literature there are different applications of this technique in the study of space (Maruskin, Scheeres, and Alfriend, 2009; Tommei, Milani, and Rossi, 2007; DeMars, Jah, and Schumacher, 2012; Farnocchia *et al*., 2010), and in the study of Earth impactors (Spoto *et al*., 2018; Valk and Lemaitre, 2006), the only examples of the method of Milani *et al.* (2004) being applied for recovery purposes are NEA 2003 BH84 (Milani *et al*., 2004) and the centaur 60558 Echeclus (Farnocchia *et al.,* 2015). Given the above, in Espitia and Quintero (2019), we extend this sample by applying the method to delimit the region of space in which a set of 6 asteroids (3 NEA, 2 MBA and 1 Hilda) were at a given date.

In this article, we present a AdRe sampling method based on the constrained Delaunay triangulation, which can establish a region of possible orbits of a minor body determined from a TSA observation. This set of orbits can determine the search area of the object in the celestial sphere for recovery purposes. Our technique does not require mesh smoothing, which reduces the computational cost.

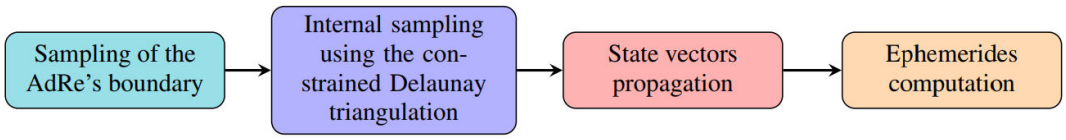

Figure-1. General scheme of the recovery procedure.

In addition, we extend the application sample of the technique of Milani et al. (2004) by determining the AdRe and applying our triangulation in the recovery of a set of 12 asteroids (6 NEA, 2 MBA, 1 Hungaria, 2 Hilda and 1 Jupiter trojan).

Based on the results obtained in this work, we discuss the capabilities and limitations of the method.

We implement our recovery technique in a web service available at http://observatorioenlinea.utp.edu.co/recoveryservice/. The source code of the algorithm is available in that same link under an open source license.

2. MATERIALS AND METHODS

2.1 Admissible Region (AdRe)

According to Milani et al. (2004), based on an attribute (Milani, 2001) given by the expression (1), the AdRe of an object is defined as the set of all possible $(\rho, \dot{\rho})$ that satisfy the following conditions:

a) The object belongs to the solar system and is not a long-orbital-period celestial body. This implies considering elliptical orbits with heliocentric energies $E_{\odot}$ less than$-k\hat{}2/2a_{max}$, with $a_{max} = 100$ AU and $k = 0.01720209895$ (Gaussian gravitational constant).

b) The object is not immersed in the Earth's gravitational field, that is, it has a geocentric energy $E_{\oplus} \geq 0$ while it is within the Earth's radius of influence ($R_{SI} = 0.010044$ AU).

$$A = (\alpha, \delta, \dot{\alpha}, \dot{\delta}) \in [-\pi, \pi) \times \left(-\frac{\pi}{2}, \frac{\pi}{2}\right) \times \mathbb{R}^2 \quad (1)$$

Condition (1) establishes the upper limit of the AdRe, which can have at most two connected components, in the extreme case in which asteroids with perihelion greater than 28 AU are studied (Spoto et al., 2018). Regarding the lower limit, according to condition (2), it is given by the curve of geocentric energy equal to zero (if $0 < \rho < R_{SI}$), or by a straight-line segment $\rho = R_{SI}$ and two arcs corresponding to the geocentric energy. It is even possible to constrain the lower limit further by ignoring the orbits belonging to meteoroids that are too small to be considered sources of meteorites. This is achieved by invoking the condition $H \leq H_{max}$ (Spoto *et al.*, 2018), with $H_{max} = 34.5$, corresponding to the threshold for meteors (Milani *et al.*, 2004).

In Espitia and Quintero (2019), we determine the AdRe's of a sample of 6 asteroids from the sets of observations that constitute TSAs, using the geocentric and topocentric variants and the logarithmic and exponential metrics. We find that the topocentric variant considerably reduces the search area of the AdRe's since it involves additional constraints, such as the exclusion of meteors. Furthermore, we find that the AdRe's that were generated from a topocentric variant have simpler geometries compared with their geocentric counterparts. Regarding the metrics, we conclude that the logarithmic metric is more adequate for analyzing the regions near the lower limit of the AdRe, whereas the exponential metric is more adequate for the regions near the upper limit. The AdRe's obtained not only excluded those bodies dominated by Earth's gravity but also considerably reduced the search area, thus optimizing the subsequent sampling from a triangulation.

3. SAMPLING OF THE AdRe (AdRe)

The diagram shown in Figure-1 summarizes the triangulation and recovery process that we implement in this work. First, we sampled the AdRe boundary through a sampling algorithm for a rectifiable curve (blue block) proposed in Milani et al. (2004). Then, we introduced a sampling strategy for the interior of the AdRe based on the constrained Delaunay triangulation (purple block). Next, we propagated all possible orbits to a later date (red block). Finally, we calculated the ephemerides for each of the propagated orbits, that is, we found the region of location of the body under study in the celestial sphere for a specific date (yellow block).

3.1 Sampling of the AdRe Boundary

According to Milani et al. (2004), the AdRe has an upper limit given by the arcs of the curve $E_{\odot}(\rho, \dot{\rho}) = 0$ or the curve $E_{\odot}(\rho, \dot{\rho}) = -k^2/2a_{max}$ (symmetric with respect to the line $\dot{\rho} = -c_1/2$). In addition, the lower limit is given by the arcs of the curve $E_{\oplus}(\rho, \dot{\rho}) = 0$ (symmetric with respect to $\dot{\rho} = 0$) and the segments of the lines $\rho = \rho_H$, $\rho = R_E$ and $\rho = R_{SI}$.

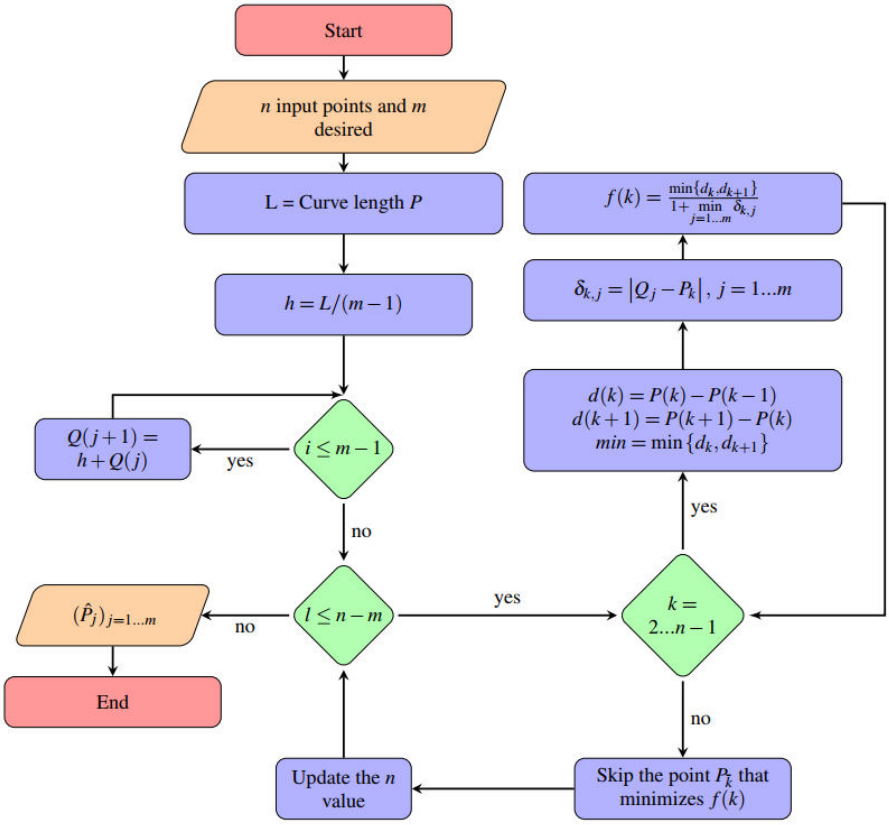

Figure-2. Algorithm for sampling the boundary of the AdRe.

The sampling of these AdRe boundaries consists of choosing points that are equispaced at the boundary, that is, if the boundary is parametrized by the arc length **s**, then the distance of each pair of consecutive points corresponds to a fixed increment of **s**. In order to avoid the calculation of **s**, Milani *et al*. (2004) proposes an algorithm that, from a large number of points equispaced on one of the 2 abscissas, applies an elimination rule that is iterated until the desired number of points at the boundary are left. The points thus obtained are close to the ideal distribution, equispaced along the arc length. The symmetry with respect to $\dot{\rho} = -c_1/2$ allows sampling the upper curve of $E_{\odot}(\rho, \dot{\rho})$ from ρ_H to the maximum value ρ_{max}. Likewise, for the sampling of the lower limit, we apply the same procedure using the symmetry with respect to $\dot{\rho} = 0$ of curve $E_{\oplus} = 0$.

Figure-2 presents the algorithm that we implement for sampling the AdRe boundary. The algorithm starts with n points of a rectifiable curve γ, with unitary length[1]. The central goal of the algorithm consists of selecting m points $(m < n)$ such that the distance along the curve between 2 consecutive points is as close as possible to $1/(m-1)$ (Milani *et al*., 2004). To avoid the calculation of the arc length **s**, we assume that γ is the unit interval $[0,1] \subset \mathbb{R}$. We then define as $(P_k)_{k=1,\dots n}$ the set of ordered points in $[0,1]$ with $P_1 = 0, P_n = 1$, and establish $(Q_j)_{j=1,\dots m}$, the sequence of ideal equispaced points with:

$$Q_{j+1} - Q_j = \frac{1}{m-1} = h \qquad ideal\ step \tag{2}$$

Considering $d_k = P_k - P_{k-1}$ and $\delta_{k,j} = |Q_j - P_k|$, note that for each P_k there is an ideal point Q_j, such that $\delta_{k,j} \leq h/2$. In order to discard a point from the set $(P_k)_{k=1,\dots n}$, we established an elimination rule, which seeks to eliminate the point such that $\bar{k}$ minimizes the following function:

$$f(k) = \frac{\min\{d_k, d_{k+1}\}}{1+\min_{j=1\dots m} \delta_{k,j}} \qquad k = 2, \dots n-1 \tag{3}$$

The process above is applied $(n-m)$ times. In each iteration, the values of d_k change due to the elimination rule of points in the set $(P_k)_{k=1,\dots n}$ given by (3). Finally, we denote by $(\hat{P}_j)_{j=1\dots m}$ the subset of points selected along the AdRe boundary. We implemented the algorithm described above in a Matlab function. Figure-3 presents the result obtained when applying this algorithm in the sampling of the AdRe boundary of asteroid 1738 Oosterhoff.

3.2 Internal Sampling of the AdRe

After the sampling of the AdRe boundary, it is necessary to sample the internal region. (Milani et al., 2004) and (Milani and Gronchi, 2009) claim that an optimum method for improving this task consists of performing a triangulation followed by mesh smoothing.

We propose a strategy based on the constrained Delaunay triangulation, which operates as follows. Given the domain of a polynomial $\widetilde{\mathcal{D}} \subset \mathcal{D}$ defined by the connection with the edges of the sample of boundary points (obtained in subsection 3.1) of the AdRe $\mathcal{D}$, the triangulation of the polygonal domain $\widetilde{\mathcal{D}}$ is the pair $(\prod, \tau)$, with $\prod = \{P_1, \ldots, P_N\}$ as the set of nodes of the domain, and $\tau = \{T_1, \ldots, T_2\}$ as the set of triangles T_i, whose vertexes are in $\prod$. This triangulation has to fulfill the following conditions:

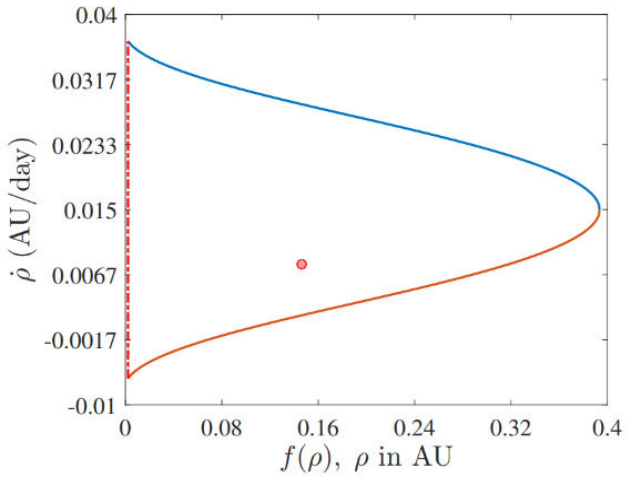

(a) AdRe using exponential metric.

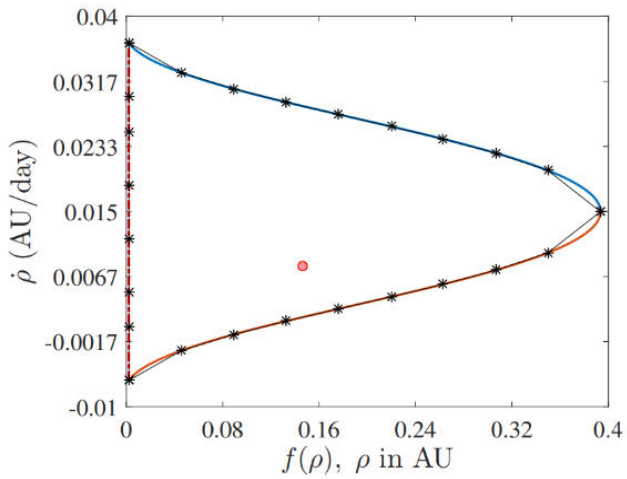

(b) AdRe sampled at its boundary.

Figure-3. Sampling of boundary of the AdRe for asteroid 1738 Oosterhoff. The red dot shows the real position of the asteroid obtained from the HORIZONS Web-Interface service of NASA's JPL.

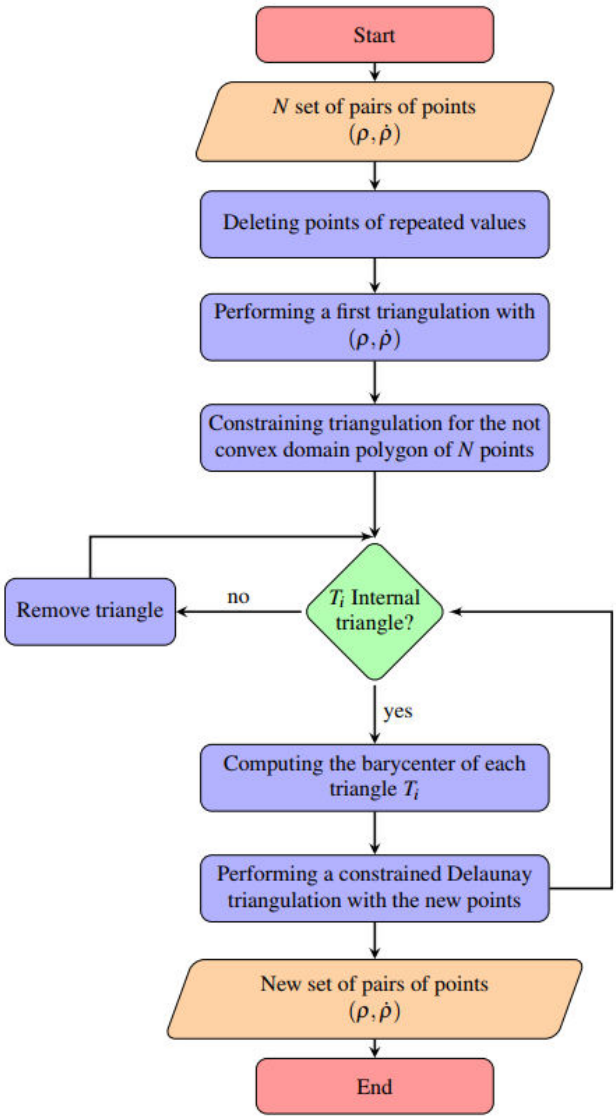

Figure-4. Constrained Delaunay triangulation algorithm for sampling inside the boundary of AdRe.

a) $\cup_{i=1,k}\ T_i = \widetilde{\mathcal{D}}$.
b) For each $i \neq j$, the set $T_i \cap T_j$ is empty, or a vertex is empty, or a side of a triangle, or one of its edges.

If in addition to the set of points $\prod$, some edges P_iP_j are entered as inputs (for example the boundary edges of $\widetilde{\mathcal{D}}^1$), the triangulation that contains the prescribed edges is called a constrained triangulation.

For each triangulation $(\prod, \tau)$, we can associate the minimum angle, which is defined as the minimum between the angles of all the triangles T_i. Among other possible triangulations of a convex domain, there is a construction called the *Delaunay triangulation* (Bern and Eppstein, 1995), which is characterized by the following properties:

a) It maximizes the minimum angle.
b) It minimizes the circumscribed circle.

c) For each triangleT_i, the internal part of its circumscribed circumference does not contain any node of the triangulation (Risler, 1992).

When they are convex domains, the previous properties are equivalent. If the domain is a convex quadrangle whose vertexes $\prod$ are not on the same circle, there are two possible triangulations $(\prod, \tau_1)$, $(\prod, \tau_2)$. According to the property (iii), only one of these triangulations is a Delaunay triangulation. In this case, the Delaunay triangulation is obtained through a first triangulation using a technique called edge-flipping (Milani and Gronchi, 2009). Note that the AdRe domain, $\widetilde{\mathcal{D}}$, is not generally convex. In this scenario, there is still a triangulation that maximizes the minimum angle, known as the constrained Delaunay triangulation, but property (iii) is not guaranteed. For each triangleT_i, a procedure is iterated over the adjacent triangles. If the common edge with the adjacent triangle is not Delaunay, the edge-flipping technique is applied. This procedure is repeated until all edges of the structure in the triangulation are Delaunay or are the edges of the boundary$\widetilde{\mathcal{D}}$. In each repetition, the minimum angle increases, and the triangulation that maximizes the minimum angle is obtained at the end (Delaunay, 1934).

In order to implement the triangulation described in the previous paragraphs, we develop an algorithm that begins by generating a constrained Delaunay triangulation $(\prod_0, \tau_0)$ with the boundary points (generated as shown in 3.1) and the boundary edges. Once the initial triangulation is obtained, it is refined by adding internal points to the domain, maintaining the Delaunay property at each intersection. In each case, a new point is added, which extends to the internal part of the discrete density domain defined in the boundary point for the quantities:

$$\rho\, P_j \;=\; \min_{l \neq j} \left| P_l \;-\; P_j \right|,$$

With the corresponding densities

$$\tilde{\rho}\, G_i \;= \frac{1}{3} \sum_{m=1}^{3} \rho\; P_{im},$$

Where G_i corresponds to the barycenters of the triangles T_i and the barycenter $G_{\bar{k}}$ is added as new point, which maximizes the minimum distance (weighted by its density$\tilde{\rho}\, G_{\bar{k}}$) from the triangulation nodes (P_{im}, $m = 1,\ldots 3$, belong to the same triangle T_i). Then, the corresponding triangle T_k is removed, and the triangles obtained by joining the edges of T_k with the new point are added to τ. Consequently, the optimum property of the Delaunay triangulation is conserved in each insertion.

The flow diagram in Figure-4 shows the procedure used for triangulating the AdRe as a domain, which is generally not convex. It begins with a number of points resulting from the sampling of the boundary (for example, $N = 25$), out of which the repeated data are removed (result of sampling the curves at its points of intersection). Then, a first triangulation is performed to identify the triangles outside the AdRe. Then, the domain is constrained, and a first constrained Delaunay triangulation is performed (the outer triangles are removed again).

The following step consists of calculating the barycenters of each triangle T_i and with them performing again a constrained Delaunay triangulation. This last step is performed twice.

The algorithm in question was implemented as a MATLAB function. Figure-5 presents the results obtained when applying our algorithm for sampling inside the AdRe boundary of asteroid 1738 Oosterhoff.

3.3 Propagation of Orbits and Ephemeris Region

Once the boundary and the internal region of the AdRe are sampled, it is necessary to propagate the established points to define the possible orbits that belong to the object under study. In fact, this object corresponds to a minor body $\mathfrak{B}$ that belongs to the solar system and that moves around the sun with heliocentric position r, which is observed from Earth $\mathcal{E}$, with a radius vector R, known for a given instant of time. As is evident, the vector between the Earth and the minor body $\boldsymbol{\rho}$ is the unknown that was solved in the previous sections. This process gives as a result a set of possible values$(\boldsymbol{\rho}, \dot{\boldsymbol{\rho}})$, for the average time of the observations collected from a TSA. Each of these points defines a virtual asteroid determined by a set of six quantities of the following form:

$$X \;= \left[\alpha, \delta, \dot{\alpha}, \dot{\delta}, \rho, \dot{\rho}\right]$$

That set is known as *attributable orbital elements* (Milani and Gronchi, 2009). The following step consists of replacing each point $(\rho, \dot{\rho})$, or node of the triangulation (after going back to its original metric), in the state vector expression defined by equation (4).

$$\begin{aligned} \mathrm{r} \;&=\; \mathrm{R} \;+ \rho\hat{\rho} \\ \dot{\mathrm{r}} \;&=\; \dot{\mathrm{R}} \;+ \dot{\rho}\hat{\rho} \;+ \rho\left(\dot{\alpha}\hat{\rho}_{\alpha} \;+ \dot{\delta}\hat{\rho}_{\delta}\right) \end{aligned} \tag{4}$$

Where $\hat{\boldsymbol{\rho}}$ is the unit vector in the direction of observation and R, $\dot{\mathrm{R}}$ is the state vector of the Earth, a parameter that is obtained from the collection times of the TSA (Espitia and Quintero, 2019), with:

$$\begin{aligned} \hat{\boldsymbol{\rho}} &= (\cos\alpha\cos\delta\,, \sin\alpha\cos\delta\,, \sin\delta) \\ \hat{\boldsymbol{\rho}}_{\alpha} &= (-\sin\alpha\cos\delta\,, \cos\alpha\cos\delta\,, 0) \\ \hat{\boldsymbol{\rho}}_{\delta} &= (-\cos\alpha\sin\delta\,, -\sin\alpha\sin\delta\,, \cos\delta) \end{aligned} \tag{5}$$

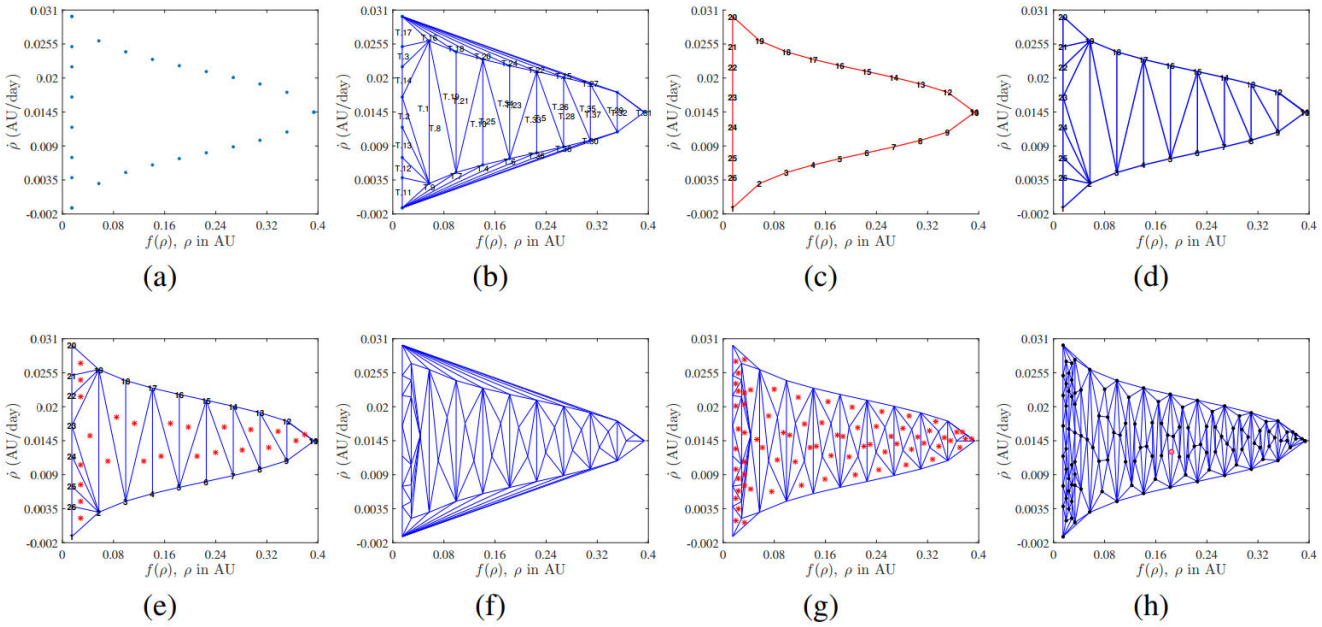

Figure-5. Results of applying our triangulation algorithm for sampling inside the AdRe boundary for asteroid 1738 Oosterhoff under the exponential metric. (a) Selection of points on the boundary. (b) First triangulation and identification of outer triangles. (c) Constraint of the AdRe domain. (d) Removal of triangles outside the domain. (e) First computation of barycenters. (f) Triangulation with the new set of points and subsequent constraint of the boundary. (g) New computation of barycenters inside the boundary of the AdRe. (h) Final result of both the boundary sampling process and constrained Delaunay triangulation. The red dot in (h) shows the asteroid real position.

As a result of this process, a set of initial state vectors $(\mathbf{r}, \dot{\mathbf{r}})$ in the heliocentric-equatorial system is obtained. We used a two-body integrator based on the functions f and g (Danby, 1962; Boulet, 1991) to obtain the set of final state vectors $(\mathbf{r_f}, \dot{\mathbf{r}}_\mathbf{f})$. Figure-6 presents this set for the case of asteroid 1738 Oosterhoff. From this set, we calculate the ephemerides, that is, the right ascension and declination coordinates for each of the points propagated for an specific date after the observation of the object under study (*ephemerides region*).

4. RESULTS AND DISCUSSIONS

We applied our recovery strategy to the set of the 12 asteroids listed in the first column of Table-1, whose types are reported in the fourth column (6 NEA, 2 MBA, 1 Hungaria, 2 Hilda and 1 Jupiter trojan). In order to achieve this goal, we use our new web recovery service available at http://observatorioenlinea.utp.edu.co/recoveryservice/.

As input data, we used the observations reported to the MPC[1] by the observatories listed in the second column within the intervals of observation presented in the third column (in all cases, the interval of observation used, constitutes a TSA). For minor bodies reported by the W63 observatory, they are registries performed by us from the Astronomical Observatory of the Technological University of Pereira, Colombia (from here on, OAUTP) exclusively for this work. The complete tables of data of the observations used in this work are available at https://www.utp.edu.co/observatorioastronomico/astrometria/recovery.

First, we established the AdRe's for the minor bodies under study following the procedure described in Espitia and Quintero (2019), using the geocentric and topocentric approximations and the exponential and logarithmic metrics.

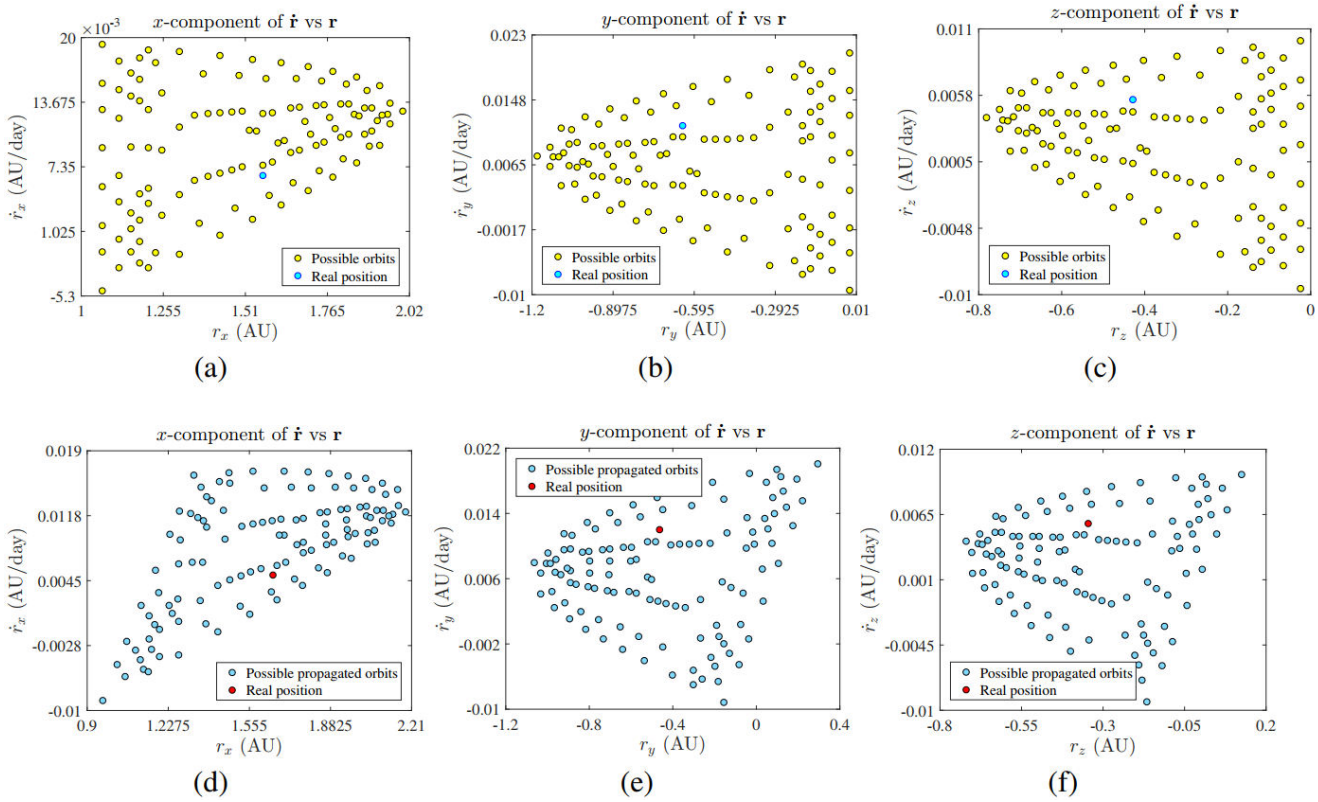

Figure-6. Components of heliocentric position and velocity vectors for asteroid 1738 Oosterhoff. Top row: vectors at the average time of initial observation. Bottom row: vectors at the recovery time. The cyan and red dots show the components of the real asteroid.

The performed tests showed that for the 12 asteroids analyzed, the most adequate version for performing an optimum sampling process was the version with topocentric correction and based on the exponential metric. This is because the topocentric approximation gives, in all cases, AdRe's with much simpler shapes than their geocentric equivalents, and the exponential metric presents a higher density of points around the asteroid's real position. Figures 7 and 8 present the AdRe's computed for the objects under study. However, we observed that the logarithmic metric describes regions of the AdRe's near the Earth with more detail, so it would be useful in the study of near meteoroids and artificial satellites. For those readers interested in these types of objects, we report the AdRe's obtained using logarithmic metrics at https://www.utp.edu.co/observatorioastronomico/astrometria/recovery.

Regarding the AdRe's calculated under the topocentric approximation and under exponential metrics, we applied the sampling technique described in section 3. Figures 9 and 10 present the results of this process. In all cases, our sampling method generated at least one node of the triangulation in the proximities of the asteroid's real position. This indicates that at least one of the ephemeris points corresponds to a value close to the asteroid's real position in the celestial sphere.

Table-1. Table of sample asteroids recovery. The observatory code, the interval of the initial observations, the orbit type, the $\mathbf{S_{max}}$ value, the proper motion, the propagated days interval and the possibility of a recovery are shown.

Asteroid	MPC Code	TSA Δt	Type	S_{max} (au) Topocen.	η (°/day)	Real Pos. ρ (au)	Propagation aprox.	Recov-ery
3122 Florence	W63	1 h 44 min	NEA/PHA	0.0849	9.3920	0.0475	12 d	no
3200 Phaethon	W63	2 h 04 min	NEA/PHA	0.2157	10.0720	0.0859	11 d 19 h	no
2003 GW	608	1 h 31 min	NEA/Apollo	1.7344	0.7996	0.9479	10 d 18 h	yes
1864 Daedalus	703	25 min 29 s	NEA/Apollo	3.5840	0.3026	1.4658	15 d 20 h	yes
2003 BH84	809	1 h 37 min	NEA/Apollo	4.4617	0.3498	1.9928	11 d 22 h	yes
1977 QQ5	F51	1 h 47 min	NEA/Amor	3.3697	0.2664	2.1336	13 d 16 h	yes
1738 Oosterhoff	W63	1 h 24 min	MBA	1.7940	0.2378	1.0104	15 d	yes
4690 Strasbourg	W63	48 min 40 s	Hungaria	2.1182	0.2916	1.3425	16 d 23 h	yes
555 Norma	W63	1 h 34 min	MBA	3.2767	0.1051	2.2395	12 d	yes
2006 SO375	705	1 h 23 min	Hilda	7.5199	0.1654	2.2756	27 d 20 h	yes
2003 GE55	291	59 min 04 s	Hilda	8.8767	0.1576	3.3645	47 d 21 h	yes
32811 Apisaon	T05	2 h 18 min	Jupiter Trojan	6.8280	0.0776	4.3549	18 d 15 h	yes

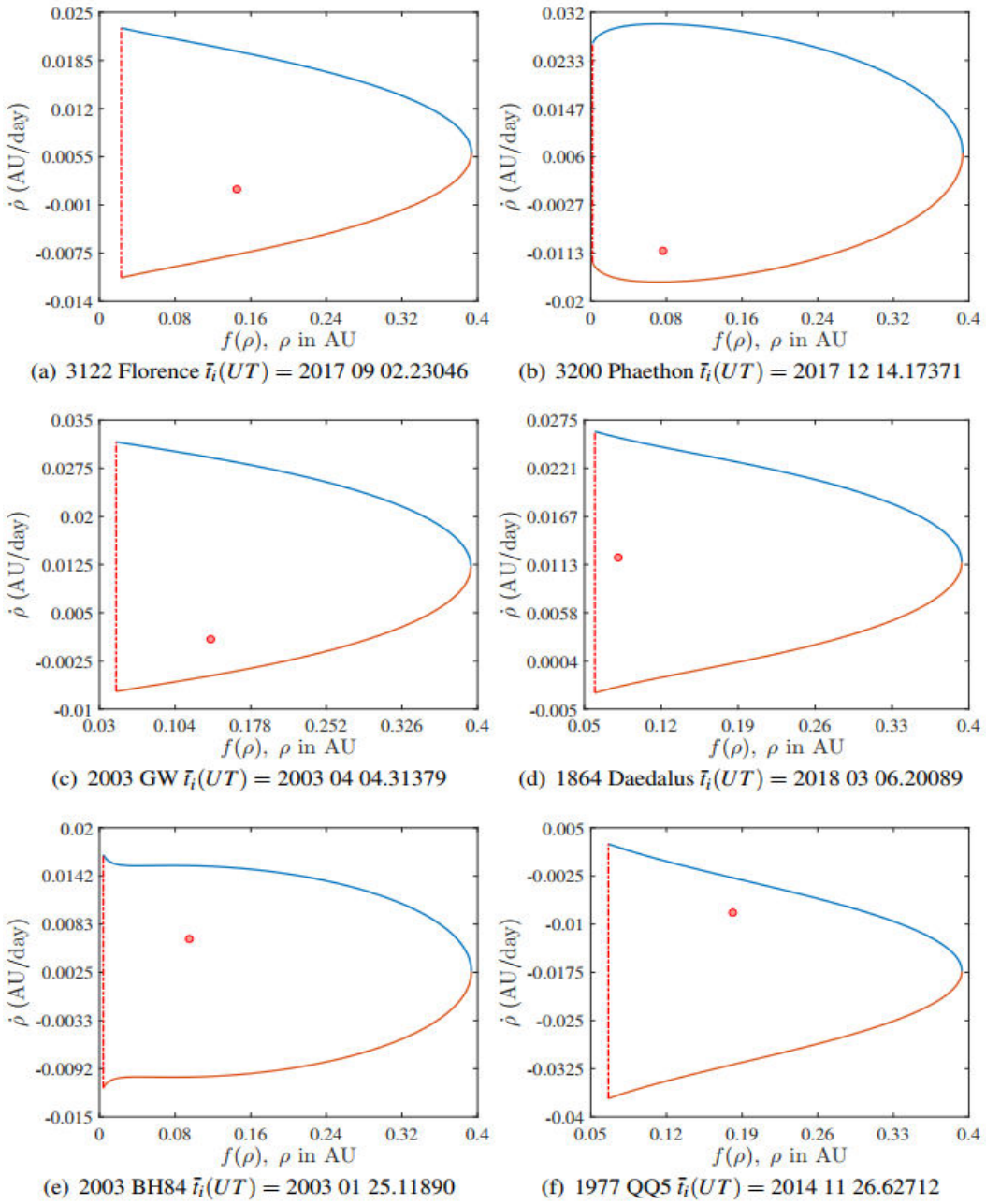

Figure-7. AdRe's for asteroids 3122 Florence, 3200 Phaethon, 2003 GW, 1864 Daedalus, 2003 BH84 and 1977 QQ5, with topocentric correction using the exponential metric. The red dot shows the real position of the asteroid obtained from the HORIZONS Web-Interface service of NASA's JPL.

We transformed each node provided by the triangulation into a heliocentric-equatorial state vector $(\boldsymbol{\rho}, \dot{\boldsymbol{\rho}})$. Then, we performed the calculation of the set of vectors for the position and velocity in the heliocentric-equatorial system $(\mathbf{r_i}, \dot{\mathbf{r}}_\mathbf{i})$. The graphs of each component for the initial times of each asteroid show that the metric that offers a cleaner sampling was the exponential one1[1]. Subsequently, we performed propagation of each of these vectors to a date after the observation (column 8, Table-1), the date at which the recovery of the asteroids in question was performed. For that purpose, we used our 2-body propagation algorithm through functions f and g. The propagation of these vectors showed that there are deformations of the AdRe's for the spatial components.

The most significant change occurred for asteroids 3200 Phaethon and 3122, whose input data were collected when they were at their points of closest approach to the Earth (the real position of the objects within their orbit at the moment of their observation is listed in the column 7 of Table-1). The changes in the shape of the AdRe's, after the propagation, become less abrupt when the asteroid is farther away from the observer.

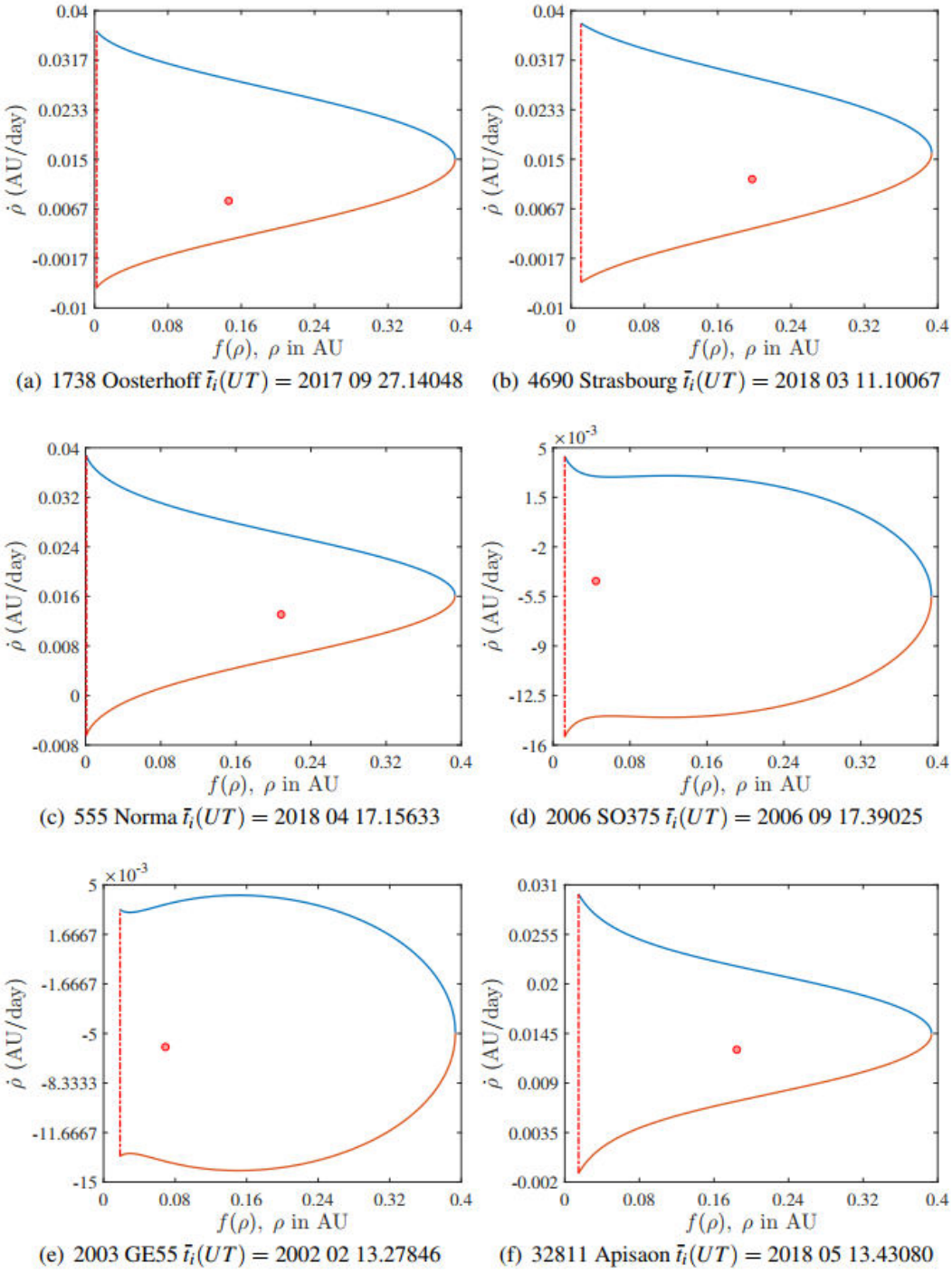

Figure-8. AdRe's for asteroids 1738 Oosterhoff, 4690 Strasbourg, 555 Norma, 2006 SO375, 2003 GE55 and 32811 Apisaon, with topocentric correction using the exponential metric. The red dot shows the real position of the asteroid obtained from the HORIZONS.

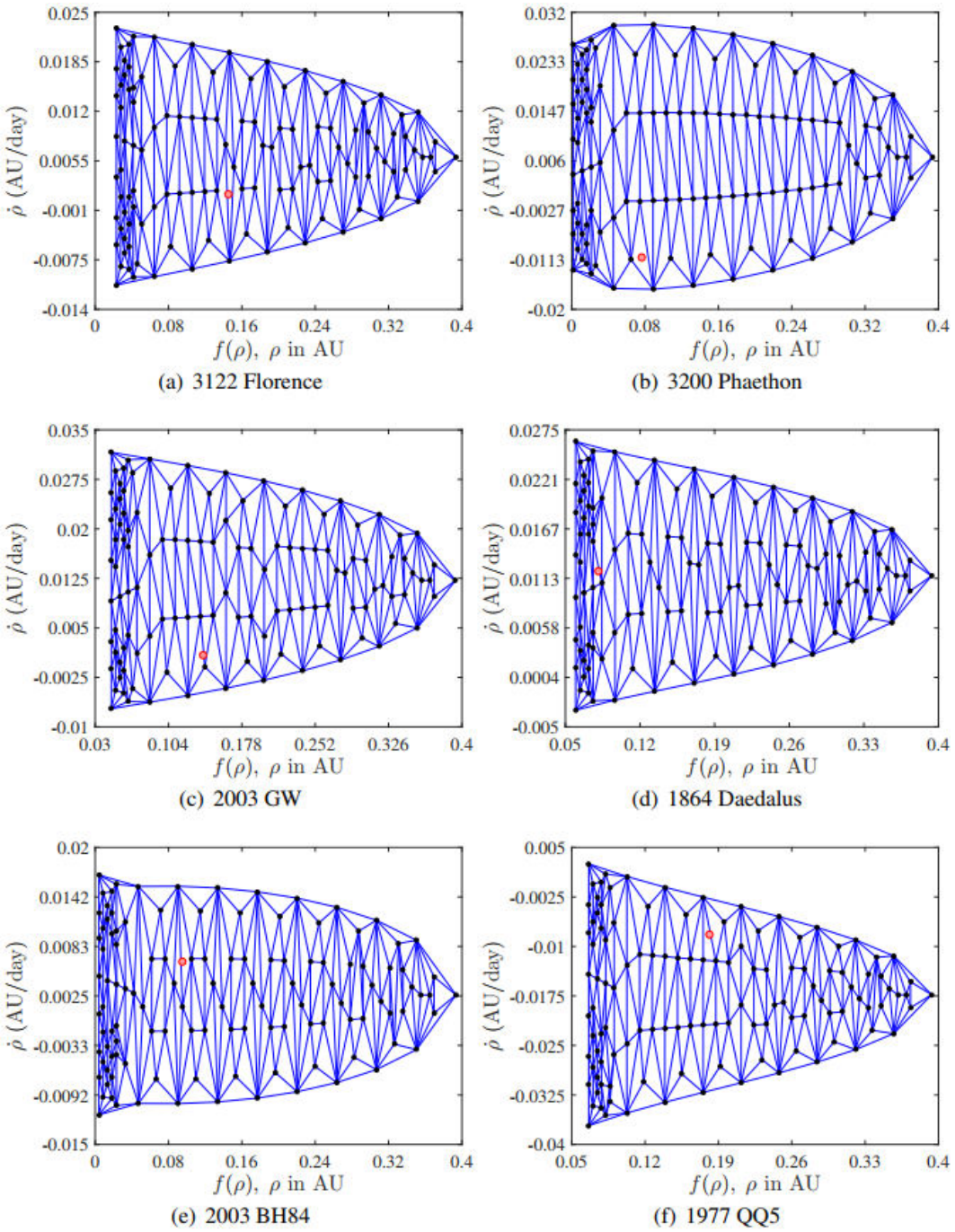

Figure-9. Triangulated AdRe's for asteroids 3122 Florence, 3200 Phaethon, 2003 GW, 1864 Daedalus, 2003 BH84 and 1977 QQ5. The red dot shows the real position of the asteroid obtained from the HORIZONS Web-Interface service of NASA's JPL.

Finally, we calculated the ephemerides for each of the points obtained from the previous process for observation times after the observations listed in column 8 of Table-1. The recovery times are calculated from the location of the OAUTP (W63). Figures 11 and 12 present the results of this process. As reference, the figures include, indicated within the blue dotted-line box, the field of vision given by the instrumental assembly of the OAUTP (95' x 72'). The asteroid's real position is also included; it was obtained from the HORIZONS Web-Interface of NASA's JPL (identified by a red dot)[1] and the recovery by Väisälä provided by the *New Object Ephemerides* service of the MPC (identified by a blue dot)[1]. The results shown in Figures 11 and 12 do not exhibit any difference when applying, for example, Laplacian mesh smoothing filter, so we concluded that our method eliminates the need for smoothing as proposed by Milani *et al.* (2004), thus increasing the computational efficiency.

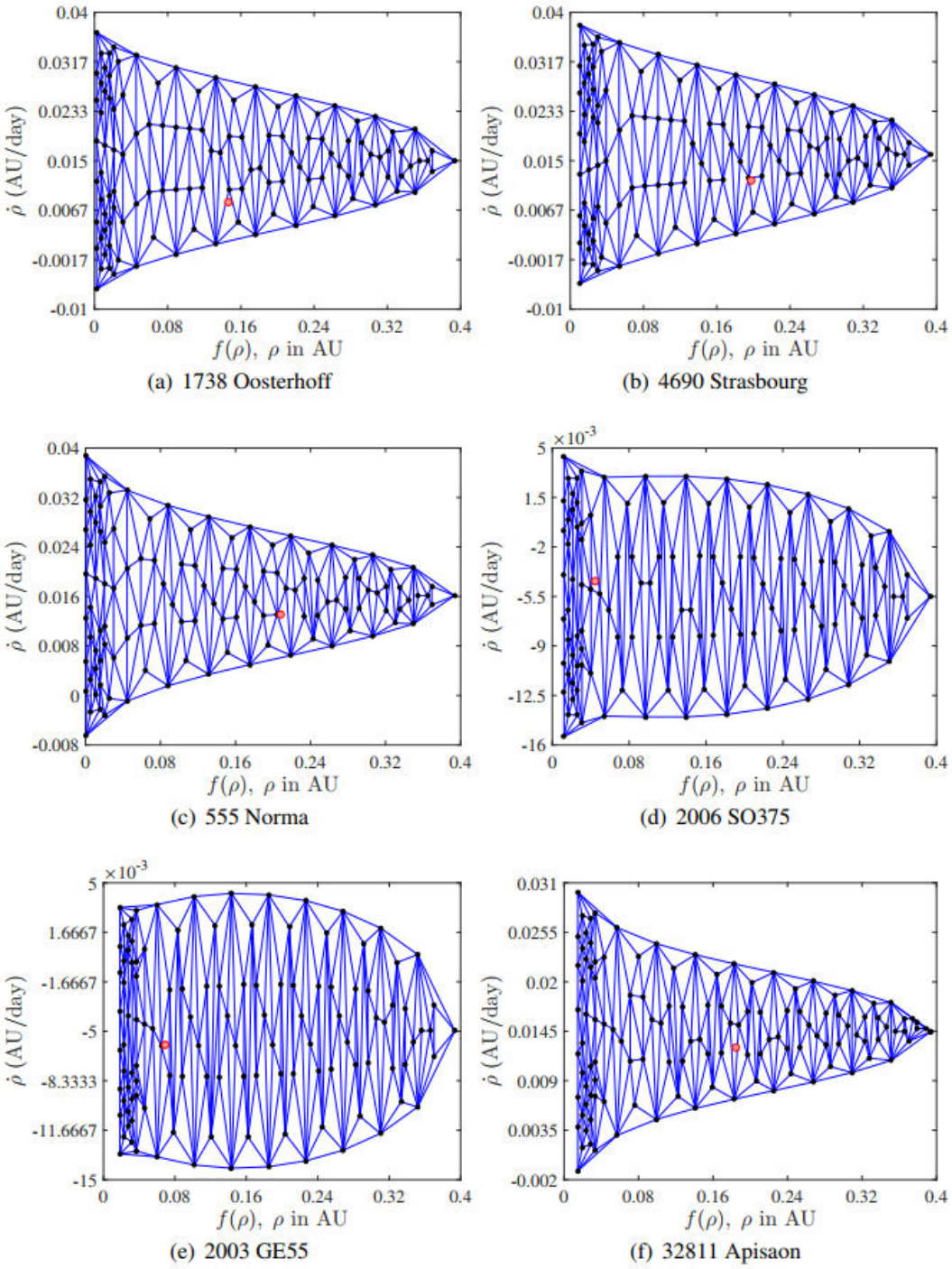

Figure-10. Triangulated AdRe's for asteroids 1738 Oosterhoff, 4690 Strasbourg, 555 Norma, 2006 SO375, 2003 GE55 and 32811 Apisaon. The red dot shows the real position of the asteroid obtained from the HORIZONS Web-Interface service of NASA's JPL.

As can be observed from Figures 11 and 12, except for asteroids 3122 Florence and 3200 Phaethon, all asteroids were recoverable, since they presented a higher density of possible location coordinates within the visual field of the OAUTP and near the asteroids' real position (red dot). In some cases, it is sufficient to recover the object again by panning the sky with a telescope that covers 3 fields of vision. Even in the cases of asteroids 2003 BH84 and 2006 SO375, our recovery was better than that provided by the New Object Ephemerides service, since our triangulated ephemerides have a higher density closer to the real position than that given by the MPC. In addition, column 8 of Table 1 shows that the recovery times range from 10 days (in the case of asteroid 2003

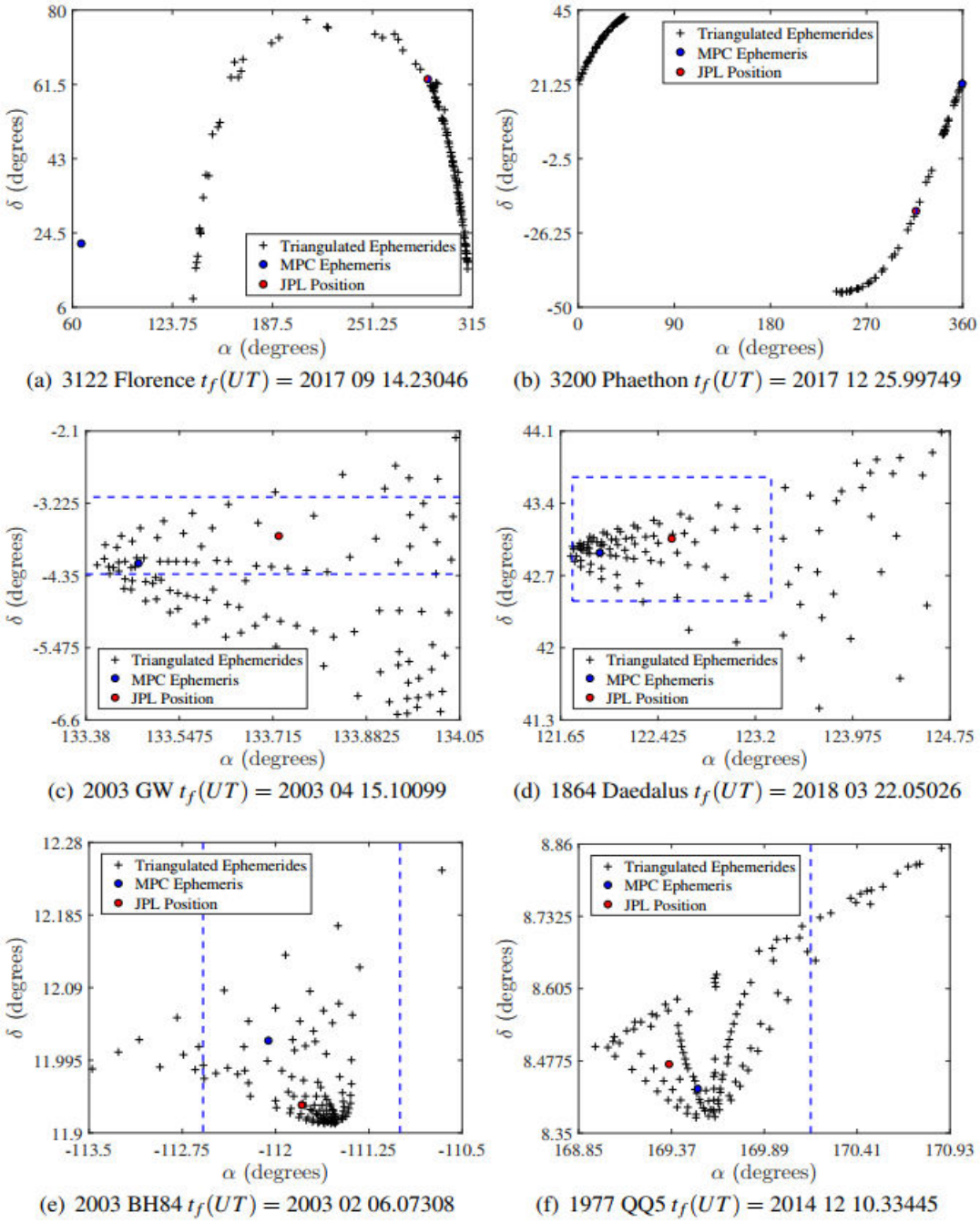

Figure-11. Ephemerides region for final date t_f for asteroids 3122 Florence, 3200 Phaethon, 2003 GW, 1864 Daedalus, 2003 BH84 and 1977 QQ5. The blue dotted lines box corresponds to the field of vision (95' x 72') given by the OAUTP instrumental assembly.

GW) up to 47 days (for the case of asteroid 2003 GE55) after the observations, from intervals of observation that do not exceed 3 hours, which demonstrates the potential of our recovery method of newly discovered objects. Our method also reduces the number of objects that inflate the lists of lost objects, since the recovery strategy would enable locating an object up to 47 days after their discovery, using an interval of observation of just 3 hours.

In the case of asteroids 3122 Florence and 3200 Phaethon, our method was not able to anticipate a recovery (last column of Table-1). In fact, the *New Object Ephemerides* service of the MPC was not able to either (see the top row of Figure-11). This was because the input observations correspond to one of the moments of closest approach to the Earth (in this case, of the order of 10^{-2} AU), and therefore their apparent motion was large (column 6 of Table-1). In the recording of a close pass by the Earth, the gravitational field can affect our propagation

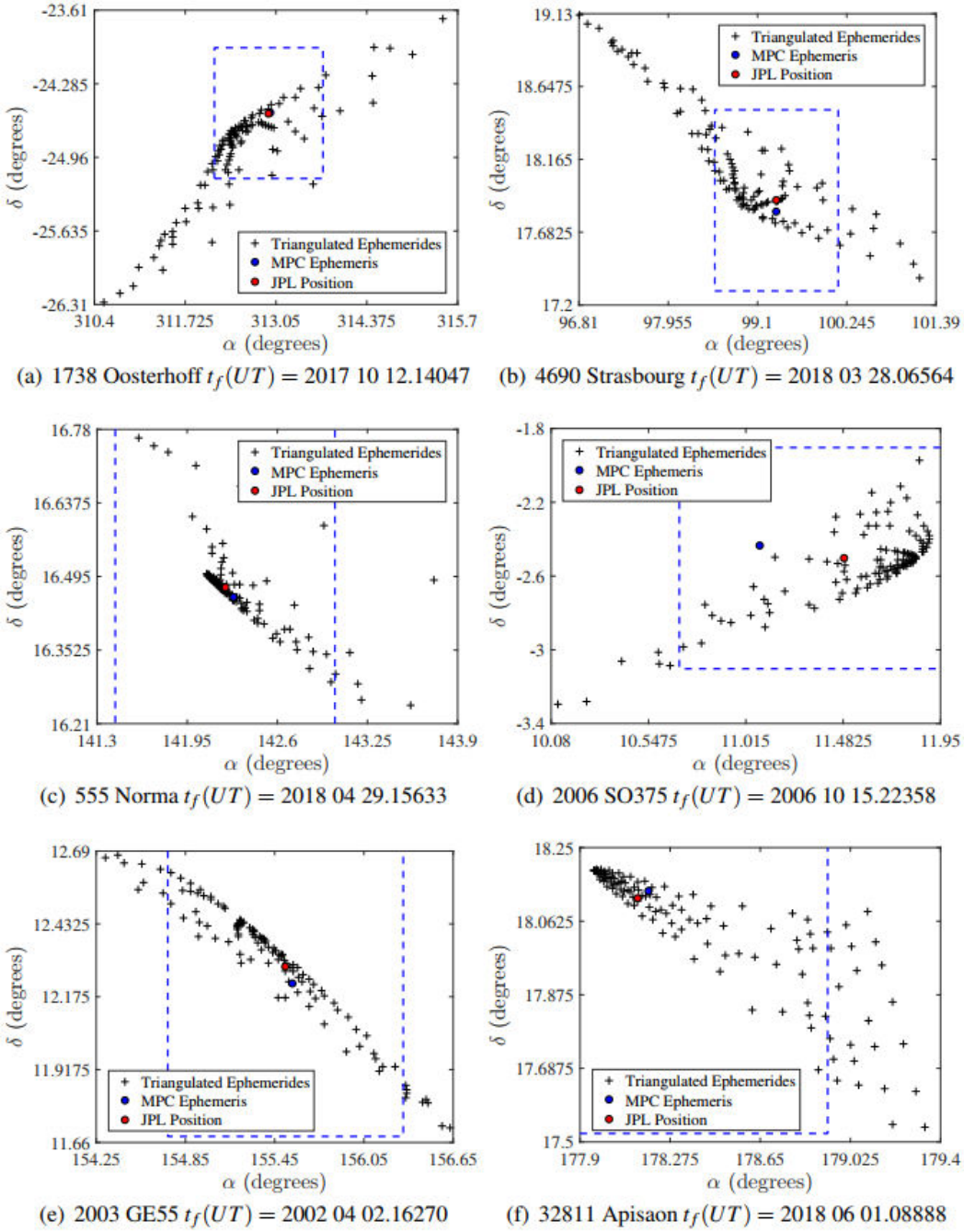

Figure-12. Ephemerides region for final date $\mathbf{t_f}$ for asteroids 1738 Oosterhoff, 4690 Strasbourg, 555 Norma, 2006 SO375, 2003 GE55 and 32811 Apisaon. The box comprised of blue dotted lines corresponds to the field of vision (95' x 72') given by the OAUTP instrumental assembly.

model based on a two-body integrator, so we conclude that in these cases, it is necessary to implement a three-body model.

In order to identify the scope of our method, we repeat the recovery of asteroid 2006 SO375, but now with just two input data separated by less than 2 minutes, corresponding to the night of their discovery (see Table 2). Figure-13 presents the ephemeris region of the asteroid for 28 days after its observation. Note how the higher density of possible positions of the asteroid provided by our algorithm (black crosses) is within the field of vision given by the instrumental assembly of the OAUTP, and closer to the real position given by the JPL's HORIZONS Web-Interface (red dot), than the recovery provided by the New Object Ephemerides service of the MPC (blue dot). This demonstrates the scopes of our technique, in addition to its application in the recovery of recently discovered minor bodies.

5. CONCLUSIONS

The literature review showed that the AdRe sampling technique is an important tool for the study of

objects (especially with short intervals of observation) that is widely applied to space debris. However, despite its versatility, we found that this technique has only been applied for recovering minor bodies in two cases: 2003 BH84 and 60558 Echeclus. In this paper, we extend the field of application of the AdRe sampling recovery technique by applying it to a group of 12 asteroids: 6 NEAs and 6 MBAs. Regarding the sampling strategy, we proposed a technique based on the constrained Delaunay triangulation, which does not require the subsequent application of a mesh smoother. In addition, we implement our recovery algorithm in a web service under an open source license. We constructed the AdRe's for the twelve asteroids from the geocentric approximation and with topocentric correction, also implementing the logarithmic and exponential metrics. The results showed that the AdRe's based on topocentric correction and using the exponential metric were better adapted to our sampling technique, since they presented a greater geometric simplicity and a higher density of possible orbits around the asteroids' real position. In addition, we observed that the AdRe's presented common elements within each family of asteroids, such that they could be used in future work to delimit the possible families to which a newly discovered object belongs.

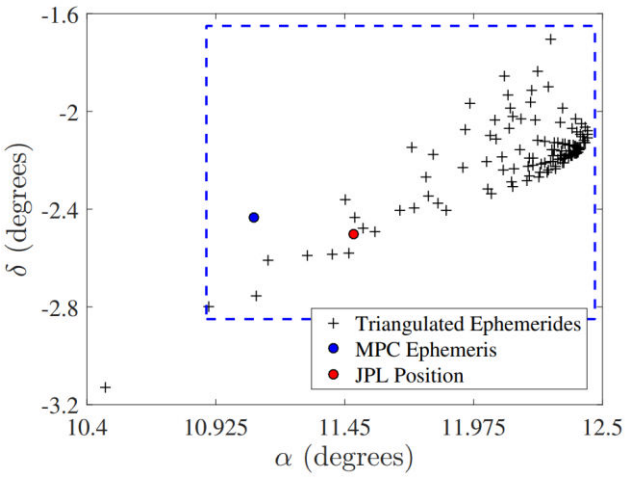

Figure-13. Ephemerides region for asteroid 2006 SO375 from 2 spaced data $\Delta t = 1$ min 11.712 s.

Table-2. Table of recovery for asteroid 2006 SO375 using an interval of $\Delta t = 1$ min 11.712 s. The initial date of observation, the recovery final date, the proper motion and the S_{max} value are shown.

Data number	TSA Δt	Initial date (UT)	Final date (UT)	η (°/day)	S_{max} AU Topocentric
2	1 min 44 11.712 s	2006 09 17.36278	2006 10 15.22358	0.1420	8.2914

For the 12 asteroids, we propagated the ephemeris region using the field of vision of the OAUTP (W63). We observed that 10 out of the 12 asteroids were recoverable, with observation times between approximately 25 minutes and 2 hours (TSA), and with propagations for recovery of up to 47 days. We even observed how with an interval of observation of just 2 minutes, it was possible to recover asteroid 2006 SO375 for approximately 28 days, which demonstrates the potential of our triangulation technique. The fact that our methodology can perform the recovery of an object, even several weeks after its observation, makes it possible for observatories exposed to changing climate conditions, as in the case of the OAUTP, to observe the object again. This enables gathering more data, which would make it possible to construct a preliminary orbit, avoiding addition of the object to the list of lost objects. In the case of asteroids 3122 Florence and 3200 Phaethon, we could not perform the recovery from the observations used as input. We concluded that this was due to these objects being at the nearest point to Earth within their orbit at the moment of observation. As can be observed from Table 1, these minor bodies had a position ρ of the order 10^{-1} AU and an average motion η much faster than the other asteroids. To validate our hypothesis, we simulated observations for this same pair of objects, but at a distance greater than 1 AU. In this case, our method did allow the recovery of the objects. The recovery that we obtained for asteroid 2003 GW ($\rho \cong 1$ AU) allows us to infer that the closer the object under study is from the Earth at the moment of observation, the more dispersed will be its ephemeris region (center-left, Figure-11). This effect could be due to its proximity to the Earth, explained by the gravitational field having a more drastic influence, which is why it would be necessary to implement a three-body model in this typ type of case.

ACKNOWLEDGMENTS

We are grateful for financial support provided by the "Vicerrectoría de Investigaciones, Innovación y Extensión" of the Universidad Tecnológica de Pereira, Colombia. This research has made use of NASA's Astrophysics Data System Bibliographic Services.

CONFLICT OF INTEREST

The authors declare that they have no conflict of interest.

REFERENCES

Bern N. and Eppstein D. 1995. Mesh generation and optimal triangulation. in Computing in Euclidean Geometry (World Scientific Publishing, Singapur) pp. 47-123.

Boulet D. L. 1991. Methods of orbit determination for the microcomputer (Willmann-Bell, Richmond) p. 565.

Danby D. M. A. 1962. Fundamentals of celestial mechanics (Macmillan Publishers, London) p. 348.

Delaunay, B. 1934. Sur la sphere vide. Izv. Akad. Nauk SSSR, Otdelenie Matematicheskii i Estestvennyka Nauk 7, 793-800.

DeMars K. J., Jah M. K. and Schumacher P. W. 2012. Initial Orbit Determination using Short-Arc Angle and Angle Rate Data. IEEE Transactions on Aerospace and Electronic Systems. 48, 2628-2637.

Espitia D. and Quintero E. A. 2019. Determination of the admissible region of asteroids with data from one night of observation. Journal of Physics: Conference Series. 1247, 1-12.

Farnocchia D., Chesley S. R., Milani A., Gronchi G. F. and Chodas P. W. 2015. Orbits, Long-Term Predictions, Impact Monitoring. in Asteroids IV (University of Arizona Press, Tucson. pp. 815-834.

Farnocchia D., Tommei G., Milani A. and Rossi A. 2010. Innovative methods of correlation and orbit determination for space debris. Celestial Mechanics and Dynamical Astronomy. 107, 169-185.

Gronchi, G. F. 2004. Classical and modern orbit determination for asteroids. Proceedings of the International Astronomical Union. 2004, 293-303.

Gwyn S. D. J., Hill N. and Kavelaars J. J. 2012. SSOS: A Moving-Object Image Search Tool for Asteroid Precovery. Publications of the Astronomical Society of the Pacific. 124, 579-585.

Kristensen L. K. 2006. Initial linking methods and their classification. Proceedings of the International Astronomical Union. 2, 301-308.

Maruskin J. M., Scheeres D. J. and Alfriend K. T. 2009. Correlation of Optical Observations of Objects in Earth Orbit. Journal of Guidance, Control, and Dynamics. 32, 194-209.

Milani A. 2001. The Asteroid Identification Problem IV: Attributions. Icarus. 151, 150-159.

Milani A. and Gronchi G. 2009. Theory of Orbit Determination (Cambridge University Press, Cambridge) p. 382.

Milani A., Gronchi G. F., Vitturi M. D. M. and Kneževi´c, Z. 2004. Orbit determination with very short arcs. I admissible regions. Celestial Mechanics and Dynamical Astronomy. 90, 57-85.

Milani A. and Knežević Z. 2005. From Astrometry to Celestial Mechanics: Orbit Determination with Very Short Arcs. Celestial Mechanics and Dynamical Astronomy. 92, 1-18.

Risler J. J. 1992. Mathematical Methods for CAD (Cambridge University Press, Cambridge) p. 198.

Spoto F., Del Vigna A., Milani A., Tommei G., Tanga P., Mignard F., Carry B., Thuillot W. and David P. 2018. Short arc orbit determination and imminent impactors in the Gaia era. Astronomy & Astrophysics. 614, 1-14.

Tommei G., Milani A. and Rossi A. 2007. Orbit determination of space debris: admissible regions. Celestial Mechanics and Dynamical Astronomy. 97, 289-304.

Väisälä Y. 1939. Eine einfache Methode der Bahnbestimmung (Suomalaisen Tiedeakatemian Kustantama) p. 32.

Valk S. and Lemaitre A. 2006. Admissible regions for too short arcs: nodal distances and elongations. Proceedings of the International Astronomical Union. 2, 455-464.